Nanoscale

PAPER

View Article Online
View Journal | View Issue

Cite this: *Nanoscale*, 2021, **13**, 9766

Enhancing multiphoton upconversion emissions through confined energy migration in lanthanide-doped Cs_2NaYF_6 nanoplatelets†

Chang Zhou,[a,b] Datao Tu, *[a,b,c] Siyuan Han,[a] Peng Zhang,[a,b] Luping Wang,[a] Shaohua Yu,[a] Jin Xu, [a,c] Renfu Li [a,c] and Xueyuan Chen *[a,b,c]

Lanthanide (Ln^{3+})-doped upconversion (UC) nanocrystals have drawn tremendous attention because of their intriguing optical properties. Currently, it is highly desired but remains challenging to achieve efficient multiphoton UC emissions. Herein, we report the controlled synthesis of a new class of UC nanocrystals based on Cs_2NaYF_6:Yb/Tm nanoplatelets (NPs), which can effectively convert the 980 nm light to five-photon and four-photon UC emissions of Tm^{3+} without the fabrication of a complicated core/multishell structure required in traditional nanocrystals. Particularly, the as-prepared Cs_2NaYF_6:Yb/Tm NPs exhibit a maximal UV-to-NIR emission intensity ratio of 1.2, which is the highest among Tm^{3+}-doped core-only UC nanocrystals. We reveal that the enhanced multiphoton UC emissions may benefit from the confined energy migration of Ln^{3+} dopants in the unique two-dimensional-like structure of Cs_2NaYF_6 NPs. As such, intense red and green UC emissions of Eu^{3+} and Tb^{3+} can further be generated *via* the cascade sensitization of Tm^{3+} and Gd^{3+} in Cs_2NaYF_6:Yb/Tm/Gd/Eu and Cs_2NaYF_6:Yb/Tm/Gd/Tb NPs, respectively. These results validate the superiority of Cs_2NaYF_6 for the future design of efficient UC nanocrystals towards versatile applications.

Received 19th March 2021,
Accepted 29th April 2021

DOI: 10.1039/d1nr01745d

rsc.li/nanoscale

Introduction

Lanthanide (Ln^{3+})-doped upconversion (UC) nanocrystals can convert low-energy excitation to high-energy emission, which makes them attractive for applications in photocatalysis, anti-counterfeiting and biosensing.[1–8] Based on the unique ladder-like 4f energy configurations of Ln^{3+} ions, UC emission from high energy levels is generated through successive absorption of low-energy photons with sensitizer ions (*e.g.*, Yb^{3+}, Nd^{3+}) and transfer of the energy to activator ions (*e.g.*, Er^{3+}, Tm^{3+}, Ho^{3+}).[9–14] Theoretically, elevating the concentration of Ln^{3+} dopants may improve the energy transfer efficiency and enhance the UC luminescence (UCL).[15,16] Unfortunately, a high concentration of dopants may cause concentration quenching of UCL due to the deleterious energy migration or cross-relaxation processes between the neighboring Ln^{3+} ions.[17,18] Moreover, the long-distance migration of excitation energy *via* highly concentrated Ln^{3+} dopants to lattice/surface defects may severely deteriorate the multiphoton UC emission in the ultraviolet (UV) spectral region.[19]

Hitherto, substantial efforts have been made to overcome such obstacles and to enhance the multiphoton UV emission in Ln^{3+}-doped UC nanocrystals.[20–22] Typically, a core/multi-shell structure has to be constructed to suppress the energy migration in traditional nanocrystals. For example, Zhou *et al.* designed $NaYF_4$:Er@$NaYbF_4$@$NaYF_4$ core/shell/shell nanocrystals to alleviate the energy back-transfer from Er^{3+} to Yb^{3+}, which promoted the three-photon UC emission of Er^{3+}.[23] Chen *et al.* synthesized $NaYF_4$@$NaYbF_4$:Tm@$NaYF_4$ core/shell/shell nanocrystals, where efficient five-photon UCL of Tm^{3+} was realized without suffering from concentration quenching of Yb^{3+}.[24] To circumvent the complicated synthesis procedures of core/multishell nanocrystals, it is of utmost importance to explore special host lattices to confine energy migration between Ln^{3+} dopants for producing intense multiphoton UC emissions.[25,26]

Cs_2NaYF_6, a face-centered cubic crystal with the space-group symmetry of $Fm\bar{3}m$, has been reported as an excellent laser or scintillation host.[27,28] In the Cs_2NaYF_6 crystal, Na^+ and Y^{3+} ions are surrounded by six halogen ions that form an

[a]*CAS Key Laboratory of Design and Assembly of Functional Nanostructures, Fujian Key Laboratory of Nanomaterials, and State Key Laboratory of Structural Chemistry, Fujian Institute of Research on the Structure of Matter, Chinese Academy of Sciences, Fuzhou, Fujian 350002, China. E-mail: dttu@fjirsm.ac.cn, xchen@fjirsm.ac.cn*
[b]*College of Chemistry, Fuzhou University, Fuzhou, Fujian 350108, China*
[c]*Fujian Science & Technology Innovation Laboratory for Optoelectronic Information of China, Fuzhou, Fujian 350108, China*

†Electronic supplementary information (ESI) available. See DOI: 10.1039/d1nr01745d

octahedron. Particularly, the unit cell parameters $a = b = c =$ 9.08 Å are much larger than those of widely reported α-$NaYF_4$ with the same space-group symmetry (unit cell parameters $a = b = c =$ 5.47 Å). As such, the energy migration between Ln^{3+} dopants is expected to be effectively confined.[29,30] So far, all the previous research studies of Ln^{3+}-doped Cs_2NaYF_6 have been carried out *via* hydrothermal and solid-state reaction methods, which resulted in bulk materials.[31,32] Nowadays, it remains a great challenge to synthesize monodisperse Ln^{3+}-doped Cs_2NaYF_6 nanocrystals, whose UCL properties and the related UC mechanism deserve to be investigated.

Herein, we propose a facile strategy for the controlled synthesis of Ln^{3+}-doped Cs_2NaYF_6 nanoplatelets (NPs). Upon excitation at 980 nm, an integrated UV-to-NIR emission intensity ratio of up to 1.2 can be achieved based on the as-prepared Cs_2NaYF_6:Yb/Tm NPs, which is ~40 times higher than that of α-$NaYF_4$:Yb/Tm counterparts. By means of structural analysis, the enhanced multiphoton UCL mechanism is attributed to the inhibition of the energy migration between Ln^{3+} dopants in Cs_2NaYF_6. Furthermore, we demonstrate that intense UC emissions of Eu^{3+} and Tb^{3+} can be generated *via* the sensitization of Tm^{3+} and Gd^{3+} in Cs_2NaYF_6:Yb/Tm/Gd/Eu and Cs_2NaYF_6:Yb/Tm/Gd/Tb NPs, respectively (Scheme 1).

Results and discussion

Cs_2NaYF_6:Yb/Tm NPs were synthesized *via* a facile high-temperature co-precipitation method, where CsF reacted with metal precursors in the mixed solvents containing oleic acid (OA), oleylamine (OAm) and octadecene (ODE) (Fig. 1a). X-ray diffraction (XRD) patterns show that all the diffraction peaks of the as-prepared NPs match well with the cubic Cs_2NaYF_6 (JCPDS no. 20-1214). Compared with those of the bulk counterparts synthesized *via* the solid-state reaction method (Fig. S1†), the XRD peaks of these NPs are broadened, indicating the smaller size of the as-prepared NPs (Fig. 1b). The growth rate of the NPs can be controlled with the reaction solvent because the ion diffusion is faster at a lower OA/OAm ratio.[33] As a result, the size of NPs can be tuned by adjusting the OA/OAm ratio. When the OA/OAm ratio decreased from 2 : 1, 1 : 1 to 1 : 2, the average size increased from 11.4 ± 1.1 nm, 16.4 ± 1.9 nm to 22.9 ± 2.9 nm (Fig. 1c–e). The thickness of the Cs_2NaYF_6:Yb/Tm NPs was determined to be 5.7 ± 0.8 nm (Fig. 1f). The high-resolution transmission electron microscopy (HRTEM) image of Cs_2NaYF_6 NPs shows clear lattice fringes (Fig. 1g). The fast Fourier transform (FFT) image of the NPs from the HRTEM image indicates that there are six nearest scattering points around each white scattering point, and the distance between them is 0.316 nm, verifying that the dominant arrangement of the synthesized Ln^{3+} doped Cs_2NaYF_6 NPs is the [111] orientation.[34] The selected-area electron diffraction (SAED) pattern of these NPs displays intense diffraction rings of cubic Cs_2NaYF_6 (Fig. 1h), confirming the pure phase and high crystallinity of the obtained NPs. In addition, the energy-dispersive X-ray (EDX) spectrum confirms the successful doping of Yb^{3+} and Tm^{3+} in Cs_2NaYF_6 NPs (Fig. S2†).

To examine the effect of Ln^{3+} dopants on UC emission, we synthesized a series of Cs_2NaYF_6:Yb/Tm NPs with different Tm^{3+} and Yb^{3+} concentrations. The optimal Tm^{3+} concentration was 1 mol%, which resulted in the maximal UCL emission upon excitation with a 980 nm laser (Fig. S3†). For Cs_2NaYF_6:*x* mol% Yb, 1 mol% Tm NPs with different Yb^{3+} concentrations (Fig. S4†), their UCL spectra consist of character-

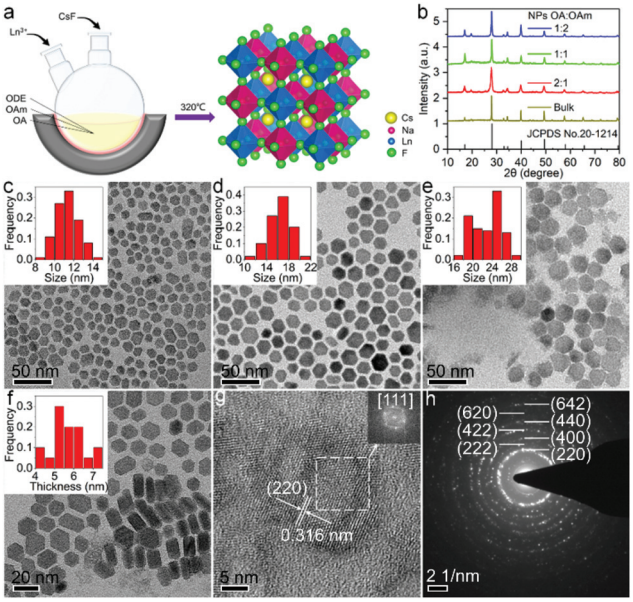

Fig. 1 (a) Schematic illustration of the synthesis of Cs_2NaYF_6:Yb/Tm NPs. (b) XRD patterns of Cs_2NaYF_6:Yb/Tm NPs and bulk materials. (c–e) Bright-field TEM images of Cs_2NaYF_6:Yb/Tm NPs synthesized with an OA/OAm ratio of 2 : 1, 1 : 1, and 1 : 2, respectively. Insets: a size distribution histogram by randomly calculating 100 particles in the TEM images. (f) Bright-field TEM images of Cs_2NaYF_6:Yb/Tm NPs synthesized with an OA/OAm ratio of 2 : 1. The inset shows the thickness distribution histogram of the as-prepared NPs. (g) HRTEM and (h) SEAD of Cs_2NaYF_6:Yb/Tm NPs.

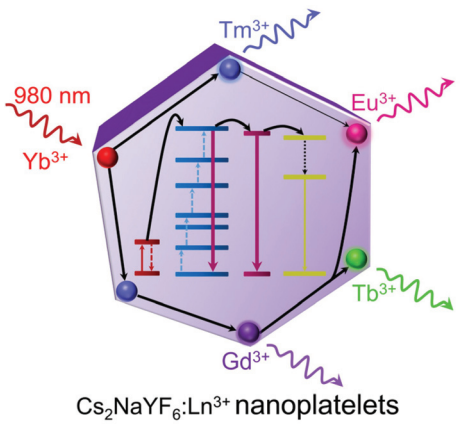

Scheme 1 Schematic illustration of Cs_2NaYF_6:Ln^{3+} NPs with highly efficient multiphoton UC emission upon 980 nm excitation.

istic sharp emission peaks which can be assigned to the five-photon $^1I_6 \rightarrow {}^3H_6$ and $^3F_4$ (290 and 348 nm), four-photon $^1D_2 \rightarrow {}^3H_6$ and $^3F_4$ (362 and 450 nm), three-photon $^1G_4 \rightarrow {}^3H_6$ and $^3F_4$ (478 and 649 nm) and two-photon $^3H_4 \rightarrow {}^3H_6$ (803 nm) transitions of Tm^{3+} (Fig. 2a). Interestingly, the five-photon and four-photon UCL emissions of Cs_2NaYF_6:Yb/Tm NPs in the UV region were observed to be strikingly strong. With the Yb^{3+} concentration of 49 mol%, a maximum integrated UV-to-NIR emission intensity ratio can be achieved (Fig. 2b).

We then compared the UCL spectra of Cs_2NaYF_6:Yb/Tm NPs and bulk materials with that of typical Tm^{3+} doped fluoride nanocrystals like α-$NaYF_4$ (Fig. 2c). Bright blue UCL can be observed for these samples upon 980 nm excitation at a power density of 150 W cm^{-2}. The absolute upconversion quantum yields for the visible and NIR regions (400–850 nm) of Cs_2NaYF_6:Yb/Tm NPs and bulk have been determined to be 0.10 ± 0.02% and 1.27 ± 0.10%, respectively, which are higher than that of α-$NaYF_4$:Yb/Tm nanocrystals (0.05 ± 0.02%). Moreover, the five-photon and four-photon UCL emissions of Cs_2NaYF_6:Yb/Tm NPs in the UV region were observed to be much stronger than those of Tm^{3+} doped α-$NaYF_4$ nanocrystals (Fig. S5†). The integrated UV-to-NIR emission intensity ratio of these samples increased with an increase in the excitation power density. With a power density of 150 W cm^{-2}, the UV-to-NIR ratios for Cs_2NaYF_6:49 mol%Yb, 1 mol%Tm NPs and bulk materials were calculated to be 1.20 and 0.51, respectively, which are ~40 and ~17 times higher than that of α-$NaYF_4$:49 mol%Yb, 1 mol%Tm nanocrystals (Fig. 2d). Note that the integrated UV-to-NIR emission intensity ratio of 1.20 is also the highest among Tm^{3+}-activated core-only UC nanocrystals (Table S1†).

As shown in Fig. 3a and b, both α-$NaYF_4$ and Cs_2NaYF_6 are face-centered cubic crystals with the space-group symmetry of $Fm\bar{3}m$. In α-$NaYF_4$ and Cs_2NaYF_6, Ln^{3+} dopants like Yb^{3+} and Tm^{3+} ions are doped to substitute for Y^{3+} ions. The nearest distance between Yb^{3+} and Tm^{3+} ions is 3.87 Å in α-$NaYF_4$ (Fig. 3a), which is much smaller relative to that in Cs_2NaYF_6 (6.42 Å, Fig. 3b). As such, the excitation energy in α-$NaYF_4$ may be easily depleted owing to the increased probability of energy migration, which does not favor the multiphoton UCL emission.[35]

We investigated the microscopic models of Cs_2NaYF_6:Yb/Tm bulk materials and NPs (Fig. 3c). For each Tm^{3+} ion in bulk Cs_2NaYF_6:Yb/Tm, there are twelve nearest neighboring Ln^{3+} ions, four of which are situated at the top, middle or bottom [001] layer, respectively. The existence of isotropically substituted Ln^{3+} ions may promote the dissipation of the excitation energy in such a three-dimensional (3D) structured crystal sublattice.[25,36,37] By contrast, the Cs_2NaYF_6:Yb/Tm nanocrystalline materials experience an anisotropic growth

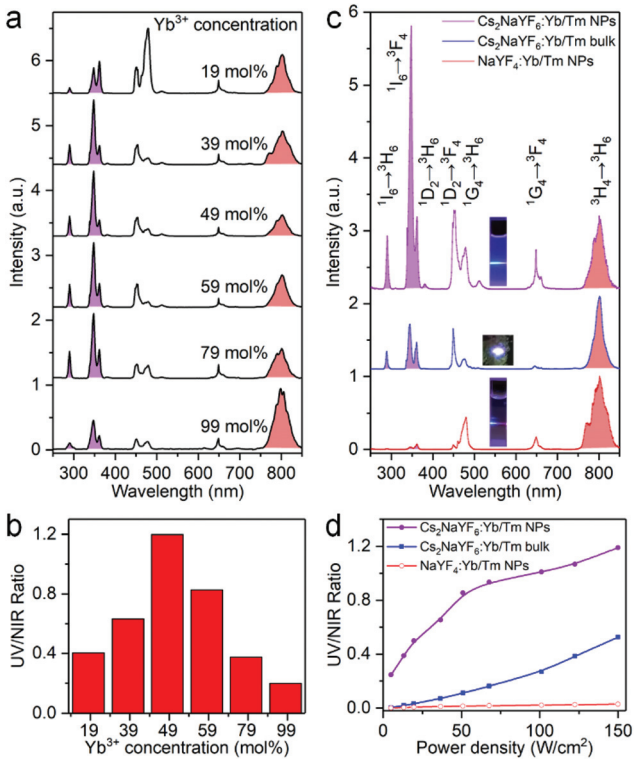

Fig. 2 (a) UC emission spectra and (b) integrated UV-to-NIR emission intensity ratio of Cs_2NaYF_6:Yb/Tm NPs with different Yb^{3+} concentrations (λ_{ex} = 980 nm, power density = 150 W cm^{-2}). (c) UC emission spectra of Cs_2NaYF_6:49 mol%Yb, 1 mol%Tm NPs, bulk and α-$NaYF_4$:49 mol%Yb, 1 mol%Tm NPs. These emission spectra were normalized at 803 nm of Tm^{3+} emission. Insets show their corresponding PL photographs. (d) Integrated UV-to-NIR emission intensity ratio in Cs_2NaYF_6:49 mol%Yb, 1 mol%Tm NPs, bulk and α-$NaYF_4$:49 mol%Yb, 1 mol%Tm NPs upon 980 nm excitation with different power densities.

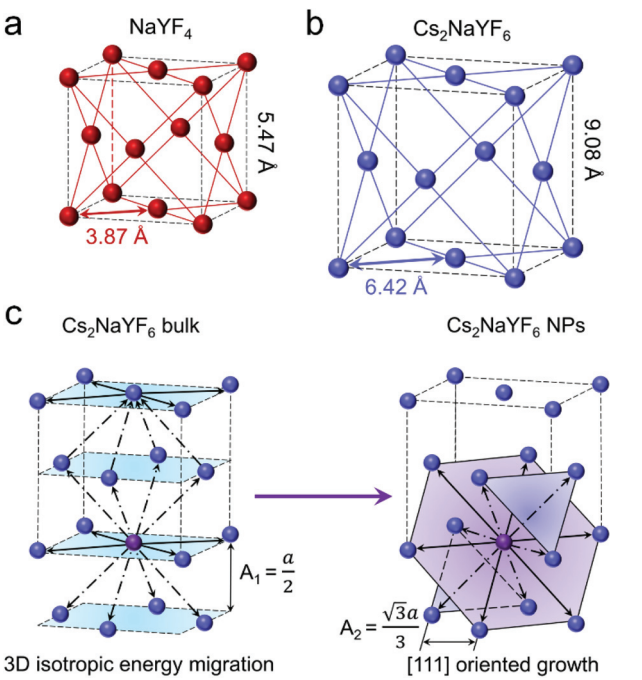

Fig. 3 Schematic illustration of the structure of (a) α-$NaYF_4$ and (b) Cs_2NaYF_6:Yb/Tm, respectively. (c) Schematic illustration of the topological energy migration pathways in Cs_2NaYF_6:Yb/Tm bulk and NPs.

along the [111] orientation (Fig. 1g), resulting in two-dimensional (2D)-like nanoplatelets. For each Tm^{3+}, six nearest neighboring Ln^{3+} ions are situated at the middle [111] layer and the other six nearest neighboring Ln^{3+} ions are situated at the top and bottom [111] layer, respectively. Moreover, the distance between two [111] layers (A_2) is calculated to be 5.24 Å, which is longer than that of two [100] layers (A_1, 4.54 Å).[38] Thus, such a 2D-like structure can effectively minimize the migration of excitation energy compared with the 3D structure,[25,39] which resulted in enhanced multiphoton UCL emission in Cs_2NaYF_6:Yb/Tm NPs relative to that in the bulk counterparts.

Besides Tm^{3+}, another Ln^{3+} ion like Gd^{3+} is often doped into inorganic nanocrystals to produce UV emission.[40] In this regard, we synthesized Cs_2NaYF_6:Yb/Tm/Gd NPs with different Gd^{3+} concentrations. EDX element mapping images indicate that the Ln^{3+} dopants are homogeneously distributed among the as-prepared NPs (Fig. S6†). Upon 980 nm excitation, a sharp UV emission peak at 311 nm can be observed, which originated from the $^6P_{7/2} \rightarrow {}^8S_{7/2}$ transition of the Gd^{3+} ion (Fig. 4a). The luminescence intensity of such UV emission increased with increasing Gd^{3+} content from 10 mol% to 30 mol%, and then decreased at higher concentrations. Meanwhile, the five-photon $^1I_6 \rightarrow {}^3H_6$ and $^3F_4$ transitions of Tm^{3+} peaking at 290 and 348 nm continuously decreased with an increase in the Gd^{3+} concentrations. Moreover, in a control experiment by replacing Cs_2NaYF_6:Yb/Tm/Gd with Cs_2NaYF_6:Yb/Gd NPs under otherwise identical conditions, negligible UCL was detected, which indicates that the luminescence of Gd^{3+} was mainly sensitized by the nearby Tm^{3+} ions.

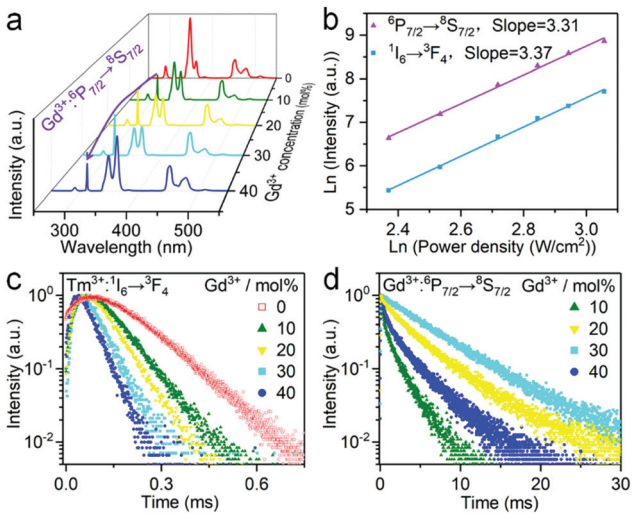

Fig. 4 (a) UC emission spectra of Cs_2NaYF_6:Yb/Tm/Gd NPs with different Gd^{3+} contents. These spectra were normalized at 450 nm of Tm^{3+} emission. (b) Ln–ln plots of the UC emission intensity *versus* excitation power density for the transitions of $^6P_{7/2} \rightarrow {}^8S_{7/2}$ of Gd^{3+} and $^1I_6 \rightarrow {}^3F_4$ of Tm^{3+} in Cs_2NaYF_6:Yb/Tm/Gd NPs, respectively. (c) PL decays of $^1I_6 \rightarrow {}^3F_4$ of Tm^{3+} and (d) $^6P_{7/2} \rightarrow {}^8S_{7/2}$ of Gd^{3+} in Cs_2NaYF_6:Yb/Tm/Gd NPs by monitoring the emissions at 348 nm and 311 nm, respectively.

To shed more light on the mechanism of the UV emission of Gd^{3+}, we obtained the UC spectra of Cs_2NaYF_6:Yb/Tm/Gd NPs excited with a 980 nm laser with different power densities. For a typical UC emission process, the value of pump photons (n) required to populate a certain emission can be determined by the relationship of $I \propto P^n$, where I and P are the UCL intensity and the pump power density, respectively. The n value for $^1I_6 \rightarrow {}^3F_4$ (348 nm) of Tm^{3+} was determined to be essentially identical to that of $^6P_{7/2} \rightarrow {}^8S_{7/2}$ (311 nm) of Gd^{3+} (Fig. 4b), which indicates that the UCL of Gd^{3+} may occur through the sensitization of the $^1I_6$ state of Tm^{3+}.

To further verify the process of energy transfer from Tm^{3+} to Gd^{3+}, we measured the UCL decays from $^1I_6$ of Tm^{3+} and $^6P_{7/2}$ of Gd^{3+} in Cs_2NaYF_6:Yb/Tm/Gd NPs. The effective lifetime of the $^6P_{7/2}$ level of Gd^{3+} increased from 1.61 ms to 7.03 ms with increasing Gd^{3+} content from 10 mol% to 30 mol%, and then decreased to 2.97 ms at higher concentrations (Fig. 4c and Table S2†). Meanwhile, the effective lifetime of the $^1I_6$ level of the Tm^{3+} ion was determined to be shortened from 163.96 μs to 50.47 μs with the increase of Gd^{3+} concentration from 0 to 40 mol% (Fig. 4d and Table S2†). All these results verified that the UCL of the $^6P_{7/2}$ state of Gd^{3+} is sensitized by the $^1I_6$ state of Tm^{3+} ions.

It has been reported that Gd^{3+} can be used as a bridge ion to sensitize a variety of Ln^{3+} ions (*e.g.*, Eu^{3+} or Tb^{3+}) without long-lived intermediate energy states to produce UC emission.[41,42] For Cs_2NaYF_6:Yb/Tm/Gd/Eu and Cs_2NaYF_6:Yb/Tm/Gd/Tb NPs, a set of new UC emission peaks appeared besides those of Tm^{3+} and Gd^{3+} upon excitation at 980 nm (Fig. 5a). These newly appeared UC emission peaks can be assigned to the $^5D_0 \rightarrow {}^7F_J$ transitions of Eu^{3+} and $^5D_4 \rightarrow {}^7F_J$ transitions of Tb^{3+}, respectively. Correspondingly, the overall UC color output turned from blue to pink or cyan, respectively (insets of Fig. 5a).

The UC mechanism responsible for the intense UCL of Eu^{3+} and Tb^{3+} in Cs_2NaYF_6 is illustrated in Fig. 5b. Upon excitation with a 980 nm laser, sensitizer ions (Yb^{3+}) absorb the pumped photons, followed by energy transfer to the neighboring Tm^{3+} to populate the $^3F_4$, $^3H_4$, $^1G_4$, $^1D_2$, and $^1I_6$ states of Tm^{3+} in sequence. Note that the energy of the $^6P_{7/2}$ level of the Gd^{3+} ion matches well with that of the $^1I_6$ level of the Tm^{3+} ion. Once the $^1I_6$ level of the Tm^{3+} ion is populated, its excitation energy will be partially transferred to the Gd^{3+} ion. The excitation energy will then be transferred to the Eu^{3+} or Tb^{3+} ion, because the $^6P_{7/2}$ level of the Gd^{3+} ion matches well with the ^5H_J level of Eu^{3+} or the ^5D_J level of Tb^{3+}. As a result, red UCL of Eu^{3+} or green UCL of Tb^{3+} can be observed. The proposed energy transfer mechanism was further confirmed by the observed UCL decays. It was determined that the photoluminescence lifetime of $^6P_{7/2}$ of Gd^{3+} was shortened from 7.03 ms to 2.83 ms, and the photoluminescence lifetime of $^1I_6$ of Tm^{3+} was shortened from 59.89 μs to 40.93 μs after the doping of Eu^{3+} (Fig. S7†).

It is worth emphasizing that two key issues contribute to the generation of efficient UCL of Eu^{3+} and Tb^{3+} in Cs_2NaYF_6:Yb/Tm/Gd/Eu and Cs_2NaYF_6:Yb/Tm/Gd/Tb NPs, respectively.

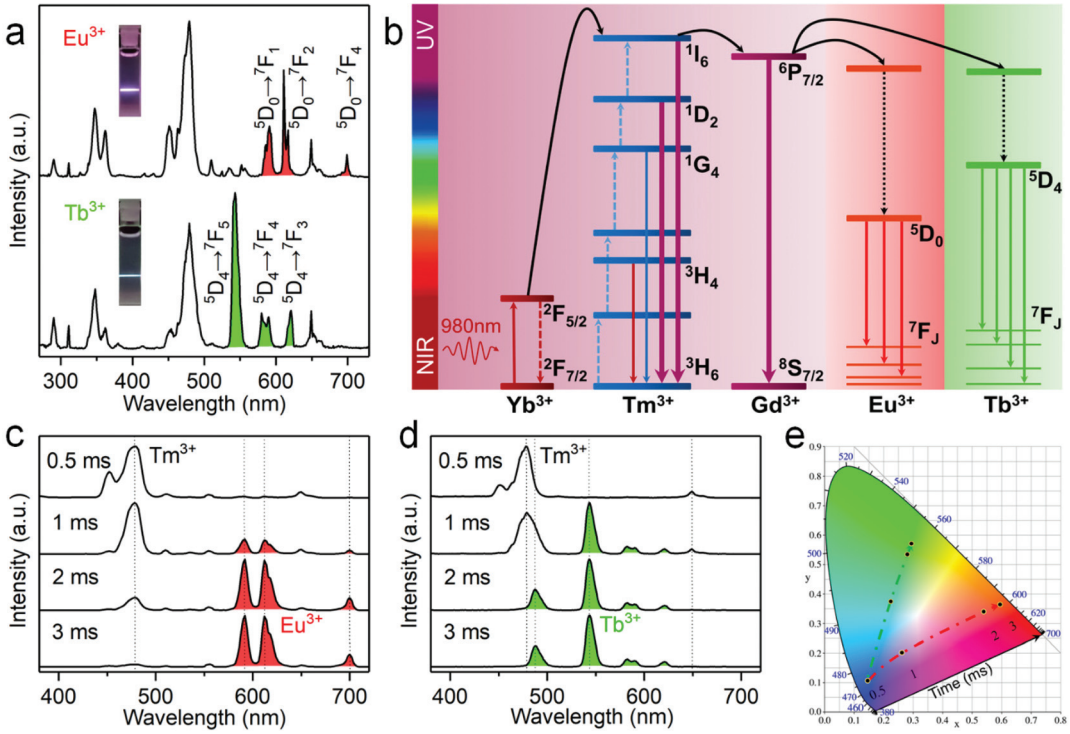

Fig. 5 (a) UCL spectra of Cs_2NaYF_6:Yb/Tm/Gd/Eu and Cs_2NaYF_6:Yb/Tm/Gd/Tb NPs dispersed in hexane upon excitation at 980 nm with a power density of 150 W cm^{-2}. Insets show their PL photographs. (b) Schematic energy level diagram showing the sensitization mechanism of Eu^{3+} (red) and Tb^{3+} (green) in Cs_2NaYF_6:Yb/Tm/Gd/Eu and Cs_2NaYF_6:Yb/Tm/Gd/Tb, respectively. The time evolution of UCL spectra for the (c) Cs_2NaYF_6:Yb/Tm/Gd/Eu and (d) Cs_2NaYF_6:Yb/Tm/Gd/Tb NPs upon excitation with a 980 nm pulse laser as the excitation source with the average power density of ~40 W cm^{-2}. (e) Corresponding CIE chromaticity coordinates for Cs_2NaYF_6:Yb/Tm/Gd/Eu (red) and Cs_2NaYF_6:Yb/Tm/Gd/Tb (green) NPs in (c) and (d), respectively.

Firstly, Gd^{3+} plays an important role as the energy transfer bridge. Without the doping of Gd^{3+}, the UCL of Eu^{3+} in Cs_2NaYF_6:Yb/Tm/Eu NPs was observed to be negligibly weak because of the large energy mismatch between the $^2F_{5/2} \rightarrow {}^2F_{7/2}$ transition of Yb^{3+} and the $^5D_J \rightarrow {}^7F_J$ transition of Eu^{3+}. As such, the UCL of Eu^{3+} cannot be efficiently sensitized by the direct energy transfer between Tm^{3+} and Eu^{3+}. By contrast, additional doping of Gd^{3+} resulted in much enhanced UCL of Eu^{3+} by ~25 times (Fig. S8†). In addition, the confined energy migration of Ln^{3+} dopants in the Cs_2NaYF_6 lattice is also critical. Note that in the previous reports regarding the generation of UCL from Eu^{3+} and Tb^{3+}, the core–shell or core–multishell structure is a prerequisite for space separation of Tm^{3+} and Eu^{3+}/Tb^{3+} so as to restrain the deleterious cross-relaxations between them.[5,41] In this work, the UCL of Eu^{3+} in Cs_2NaYF_6:Yb/Tm/Gd/Eu NPs can be markedly enhanced by ~38 times that of traditional fluorides like α-$NaYF_4$:Yb/Tm/Gd/Eu nanocrystals (Fig. S8†). To the best of our knowledge, such an efficient UCL of Eu^{3+} or Tb^{3+} in Cs_2NaYF_6 NPs has not been realized in other Eu^{3+} or Tb^{3+}-doped core-only nanocrystals before.

As shown in Fig. 5a, the pure UCL of Eu^{3+} or Tb^{3+} cannot be obtained directly using the steady-state luminescence mode. The effective lifetimes of the $^5D_0$ level of Eu^{3+} and the $^5D_4$ level of Tb^{3+} in Cs_2NaYF_6 NPs have been determined to be 2.60 ms and 2.25 ms, respectively (Fig. S9†), which are about two orders of magnitude longer than those of Tm^{3+} in these NPs (Fig. S7†). By virtue of the large difference in the UC luminescence lifetime between Eu^{3+}/Tb^{3+} and Tm^{3+} ions, it is easy to separate their UCL based on the time-resolved detection technique by setting an appropriate delay time and gate time. Fig. 5c and d show the time-resolved UCL spectra of Cs_2NaYF_6:Yb/Tm/Gd/Eu and Cs_2NaYF_6:Yb/Tm/Gd/Tb NPs, respectively. Their UCL spectra were dominated by the emission of Tm^{3+} when the delay time was within 1 ms. When the delay time is longer than 3 ms, pure red UCL attributed to the $^5D_0 \rightarrow {}^7F_J$ (J = 1, 2, 3, and 4) transition of the Eu^{3+} ion and green UCL attributed to the $^5D_4 \rightarrow {}^7F_J$ (J = 3, 4, 5, and 6) transition of Tb^{3+} were observed, respectively. As revealed by their corresponding CIE chromaticity coordinates (Fig. 5e), the UC color changed from blue to red or green for Cs_2NaYF_6:Yb/Tm/Gd/Eu or Cs_2NaYF_6:Yb/Tm/Gd/Tb NPs, respectively. Such an intriguing time-dependent UCL color output in Ln^{3+}-doped Cs_2NaYF_6 NPs is favorable for potential applications such as in time-resolved bioimaging and multilevel anti-counterfeiting.

Conclusions

In summary, we have developed a new class of Ln^{3+}-doped Cs_2NaYF_6 NPs without a core/shell structure to achieve highly

efficient multiphoton UCL emissions. Upon excitation at 980 nm, intense UV emissions of Tm^{3+} were realized in Cs_2NaYF_6:Yb/Tm NPs by virtue of the large distance between the adjacent Ln^{3+} dopants in the host lattice. The optimal UV-to-NIR emission intensity ratio of Cs_2NaYF_6:Yb/Tm NPs has been determined to be 1.2, which is the highest among Tm^{3+}-activated core-only UC nanocrystals. Moreover, intense UV emission of Gd^{3+} has been realized in Cs_2NaYF_6:Yb/Tm/Gd NPs *via* the energy transfer from Tm^{3+} to Gd^{3+}. Particularly, we have demonstrated that bright red and green UC emissions of Eu^{3+} and Tb^{3+} can be generated *via* the cascade sensitization of Tm^{3+} and Gd^{3+} in Cs_2NaYF_6:Yb/Tm/Gd/Eu and Cs_2NaYF_6:Yb/Tm/Gd/Tb NPs, respectively. These findings reveal the great potential of tuning UCL emissions in Ln^{3+}-doped Cs_2NaYF_6 NPs, which may open up a promising avenue for the exploitation of Ln^{3+}-doped nanocrystals with excellent optical properties for versatile applications.

Experimental

Detailed experimental procedures are reported in the ESI.†

Author contributions

C. Z. prepared samples and collected data for the original draft. S.Y. H. and P. Z. assisted in PL measurements. L.P. W., S. H. Y., J. X. and R.F. L. contributed to conceptualization and investigation. C. Z., D.T. T. and X.Y. C. prepared the manuscript.

Conflicts of interest

There are no conflicts to declare.

Acknowledgements

This work was supported by the Science and Technology Cooperation Fund between Chinese and Australian Governments (2017YFE0132300), the Strategic Priority Research Program of the CAS (XDB20000000), the NSFC (no. U1805252, 21975257, 21771185, 12074380, and 11704380), and the CAS/SAFEA International Partnership Program for Creative Research Teams, NSF of Fujian Province (no. 2019I0029).

Notes and references

1 M. L. Deng, Y. X. Ma, S. Huang, G. F. Hu and L. Y. Wang, *Nano Res.*, 2011, **4**, 685–694.
2 B. Zhou, B. Shi, D. Jin and X. Liu, *Nat. Nanotechnol.*, 2015, **10**, 924–936.
3 D. Li, S. H. Yu and H. L. Jiang, *Adv. Mater.*, 2018, **30**, 1707377.
4 W. J. Yao, Q. Y. Tian, B. Tian, M. X. Li, H. J. Wang, P. Zeng, L. Liu, H. Zheng and W. Wu, *Sci. China Mater.*, 2019, **62**, 368–378.
5 M. Ding, B. Dong, Y. Lu, X. Yang, Y. Yuan, W. Bai, S. Wu, Z. Ji, C. Lu and K. Zhang, *Adv. Mater.*, 2020, **32**, 2002121.
6 N. Xin, D. Wei, Y. Zhu, M. Yang, S. Ramakrishna, O. Lee, H. Luo and H. Fan, *Mater. Today Chem.*, 2020, **17**, 100329.
7 J. K. Chen, S. X. Wang, J. D. Lin and D. Q. Chen, *Nanoscale*, 2019, **11**, 22359–22368.
8 H. Huang, J. K. Chen, Y. T. Liu, J. D. Lin, S. X. Wang, F. Huang and D. Q. Chen, *Small*, 2020, **16**, 12.
9 F. Wang, Y. Han, C. S. Lim, Y. Lu, J. Wang, J. Xu, H. Chen, C. Zhang, M. Hong and X. Liu, *Nature*, 2010, **463**, 1061–1065.
10 C. Zhang, L. D. Sun, Y. W. Zhang and C. H. Yan, *J. Rare Earths*, 2010, **28**, 807–819.
11 S. Gai, C. Li, P. Yang and J. Lin, *Chem. Rev.*, 2014, **114**, 2343–2389.
12 W. Luo, Y. Liu and X. Chen, *Sci. China Mater.*, 2015, **58**, 819–850.
13 X. W. Zhang, Z. Zhao, X. Zhang, D. B. Cordes, B. Weeks, B. S. Qiu, K. Madanan, D. Sardar and J. Chaudhuri, *Nano Res.*, 2015, **8**, 636–648.
14 Q. Zou, P. Huang, W. Zheng, W. You, R. Li, D. Tu, J. Xu and X. Chen, *Nanoscale*, 2017, **9**, 6521–6528.
15 J. Shen, G. Chen, T. Y. Ohulchanskyy, S. J. Kesseli, S. Buchholz, Z. Li, P. N. Prasad and G. Han, *Small*, 2013, **9**, 3213–3217.
16 A. Punjabi, X. Wu, A. Tokatli-Apollon, M. El-Rifai, H. Lee, Y. Zhang, C. Wang, Z. Liu, E. M. Chan and C. Duan, *ACS Nano*, 2014, **8**, 10621–10630.
17 S. Wen, J. Zhou, K. Zheng, A. Bednarkiewicz, X. Liu and D. Jin, *Nat. Commun.*, 2018, **9**, 2415.
18 B. Chen and F. Wang, *Acc. Chem. Res.*, 2019, **53**, 358–367.
19 L. Tu, X. Liu, F. Wu and H. Zhang, *Chem. Soc. Rev.*, 2015, **44**, 1331–1345.
20 L. Zhao, J. Peng, Q. Huang, C. Li, M. Chen, Y. Sun, Q. Lin, L. Zhu and F. Li, *Adv. Funct. Mater.*, 2014, **24**, 363–371.
21 Q. S. Chen, X. J. Xie, B. L. Huang, L. L. Liang, S. Y. Han, Z. G. Yi, Y. Wang, Y. Li, D. Y. Fan, L. Huang and X. G. Liu, *Angew. Chem., Int. Ed.*, 2017, **56**, 7605–7609.
22 S. Mei, J. Zhou, H. T. Sun, Y. Cai, L. D. Sun, D. Jin and C. H. Yan, *Adv. Sci.*, 2021, 2003325.
23 B. Zhou, B. Tang, C. Zhang, C. Y. Qin, Z. J. Gu, Y. Ma, T. Y. Zhai and J. N. Yao, *Nat. Commun.*, 2020, **11**, 1174.
24 X. Chen, L. M. Jin, W. Kong, T. Y. Sun, W. F. Zhang, X. H. Liu, J. Fan, S. F. Yu and F. Wang, *Nat. Commun.*, 2016, **7**, 10304.
25 J. Wang, R. Deng, M. A. MacDonald, B. Chen, J. Yuan, F. Wang, D. Chi, T. S. A. Hor, P. Zhang and G. Liu, *Nat. Mater.*, 2014, **13**, 157–162.
26 L. Marciniak, W. Strek, A. Bednarkiewicz, A. Lukowiak and D. Hreniak, *Opt. Mater.*, 2011, **33**, 1492–1494.
27 T. Pawlik and J. M. Spaeth, *J. Appl. Phys.*, 1997, **82**, 4236–4240.

28 V. N. Makhov, N. M. Khaidukov, D. Lo, J. C. Krupa, M. Kirm and E. Negodin, *Opt. Mater.*, 2005, **27**, 1131–1137.
29 P. A. Loiko, N. M. Khaidukov, J. Mendez-Ramos, E. V. Vilejshikova, N. A. Skoptsov and K. V. Yumashev, *J. Lumin.*, 2016, **175**, 260–266.
30 P. A. Loiko, E. V. Vilejshikova, N. M. Khaidukov, J. Mendez-Ramos, X. Mateos and K. V. Yumashev, *J. Lumin.*, 2017, **185**, 279–285.
31 P. A. Tanner, Y. L. Liu, N. M. Edelstein, K. M. Murdoch and N. M. Khaidukov, *J. Phys.: Condens. Matter*, 1997, **9**, 7817–7836.
32 Y. M. Yang, Z. Y. Li, J. Y. Zhang, Y. Lu, S. Q. Guo, Q. Zhao, X. Wang, Z. J. Yong, H. Li, J. P. Ma, Y. Kuroiwa, C. Moriyoshi, L. L. Hu, L. Y. Zhang, L. R. Zheng and H. T. Sun, *Light: Sci. Appl.*, 2018, **7**, 11.
33 J. Gu, Z. Q. Zhao, Y. Ding, H. L. Chen, Y. W. Zhang and C. H. Yan, *J. Am. Chem. Soc.*, 2013, **135**, 8363–8371.
34 W. Lee, D. Choi and S. Kim, *Chem. Mater.*, 2020, **32**, 6864–6874.
35 O. Malta, *J. Non-Cryst. Solids*, 2008, **354**, 4770–4776.
36 H.-X. Mai, Y.-W. Zhang, R. Si, Z.-G. Yan, L.-d. Sun, L.-P. You and C.-H. Yan, *J. Am. Chem. Soc.*, 2006, **128**, 6426–6436.
37 G. Wang, Q. Peng and Y. Li, *J. Am. Chem. Soc.*, 2009, **131**, 14200–14201.
38 K. Momma and F. Izumi, *J. Appl. Crystallogr.*, 2011, **44**, 1272–1276.
39 T. C. Ozawa, K. Fukuda, K. Akatsuka, Y. Ebina and T. Sasaki, *Chem. Mater.*, 2007, **19**, 6575–6580.
40 V. Mahalingam, R. Naccache, F. Vetrone and J. A. Capobianco, *Chem. – Eur. J.*, 2009, **15**, 9660–9663.
41 F. Wang, R. Deng, J. Wang, Q. Wang, Y. Han, H. Zhu, X. Chen and X. Liu, *Nat. Mater.*, 2011, **10**, 968–973.
42 X. Chen, D. Peng, Q. Ju and F. Wang, *Chem. Soc. Rev.*, 2015, **44**, 1318–1330.